

IRAS 22036+5306: an Al₂O₃ oxide-dominated post-AGB star

M. M. Maldoni,¹*† T. R. Ireland¹* and G. Robinson²*

¹Research School of Earth Sciences, The Australian National University, Canberra ACT 0200, Australia

²School of Physical, Environmental and Mathematical Sciences, The University of New South Wales,

Australian Defence Force Academy, Canberra ACT 2600, Australia

Accepted 2008 March 7. Received 2008 March 6; in original form 2007 June 21

ABSTRACT

Radiative transfer modelling of the *Infrared Space Observatory (ISO)* spectrum of IRAS 22036+5306 has shown that its unusual 11- μ m band can be suitably modelled with an alumina-olivine mixture substantially dominated by the former. The results of this work add further credence to recent findings that significant amounts of Al₂O₃ dust grains are present in the dust shells of stars near or beyond the tip of the asymptotic giant branch. Indeed, in the case of IRAS 22036+5306, Al₂O₃ dominates the dust composition to the extent that it shifts the 9.8- μ m band due to amorphous silicates to 11 μ m. IRAS 22036+5306 may be an unusual case in that the inner dust torus is maintained at a sufficiently high temperature for Al₂O₃ condensation, but not silicate.

Key words: radiative transfer – stars: AGB and post-AGB – circumstellar matter – dust, extinction – infrared: stars.

1 INTRODUCTION

Main-sequence stars with initial masses between 1 and 8 M_{\odot} evolve into asymptotic giant branch (AGB) stars. These are cool, luminous red giants characterized by mass-loss rates ranging from 10^{-7} up to $10^{-4} M_{\odot} \text{ yr}^{-1}$ as the star evolves along the AGB branch through the superwind phase. The superwind begins when the star becomes very luminous ($\gtrsim 4 \times 10^3 L_{\odot}$) and is driven primarily by stellar pulsations caused by thermal pulses in the star, along with dust formation (Wood, private communication; Vassiliadis & Wood 1993). It is a low velocity (10–25 km s^{-1}) but dense wind giving rise to very high mass-loss rates of up to $\sim 10^{-4} M_{\odot} \text{ yr}^{-1}$. This leads to the formation of a spherically symmetric thick dust cocoon which can completely obscure the star. Following this, an axisymmetric mass-loss process begins heralding the transition to the post-AGB or protoplanetary nebula (PPN) phase. Evidence has recently been presented indicating that this axisymmetric mass-loss may, in fact, begin in the late AGB phase (Dijkstra & Speck 2006). When the mass of the stellar envelope declines to less than about 0.01 M_{\odot} large-scale mass-loss ceases and the star begins to evolve, contracting at constant luminosity and becoming hotter, and therefore evolving towards the blue side of the Hertzsprung–Russell (HR) diagram (Kwok 1993). The star subsequently evolves into a planetary nebula (PN) as further contractions induce a stellar core temperature high enough to produce large amounts of ultraviolet (UV) photons that ionize the ejected AGB gas envelope (Kwok 1993).

Expansion of the gas envelope leads to cooling and condensation of the gas into dust grains and to the formation of circumstellar dust shells around AGB stars (Tielens 1990; Lodders & Fegley 1999). Assuming a gas of solar composition, the first major condensate is Al₂O₃ grains, which can serve as nucleation sites for subsequent condensation of silicate grains, or react with the gas so that Al₂O₃ is incorporated into lower temperature phases (e.g. melilite var. gehlenite Ca₂Al₂Si₂O₇). In either case, Al₂O₃-bearing grains become coated with other silicate species (especially olivine var. forsterite Mg₂SiO₄) and this significantly attenuates the characteristic Al₂O₃ spectral signature. It is also recognized that thermodynamic equilibrium only plays a role in the high temperature/high dust density regions closer to the star, with kinetics expected to predominate thereafter. Therefore, the theoretical condensation sequence of Tielens (1990) could conceivably freeze out at any stage of the expected condensation scheme, leading to the formation of only a partial representation of the predicted species (see fig. 1 in Tielens 1990).

Alternative non-equilibrium condensation models (Stencel et al. 1990) and Nuth & Hecht (1990) envisage the formation of ‘chaotic’ silicates or smokes. In these schemes, the early formation of Al–O bonds is included in the chaotic silicate matrix, generating a corresponding spectral band. Subsequently, upon depletion of all available Al, the initial Al–O spectral signature is overwhelmed by the 10- μ m band due to Si–O bonds.

In addition to Al₂O₃ dust (or at least dust containing Al–O bonds), there is also observational evidence in shells of low mass-loss O-rich stars for Ca–Al, Mg–Al and Mg–Fe oxides (Posch et al. 2003). As remarked by Posch et al. (2003), some stars exhibiting spectral bands of oxides show little or no amorphous silicate bands, leading them to surmise ‘whether there exists a class (or an

*E-mail: marco.maldoni@ga.gov.au (MMM); trevor.ireland@anu.edu.au (TRI); g.robinson@adfa.edu.au (GR)

†Present address: Geoscience Australia, Canberra ACT 2601, Australia.

evolutionary stage) of low mass-loss stars dominated by oxides and not silicates'. We note that DePew, Speck & Dijkstra (2006) have run extensive models for oxygen-rich AGB stars using corundum ($\alpha - \text{Al}_2\text{O}_3$), spinel (MgAl_2O_4) and silicates in an attempt to find the source of the 13- μm feature in these objects. On the basis of their modelling, they concluded that the case for corundum as the carrier of the 13- μm feature, while not proven, was strengthened. In contrast, in this paper we use amorphous Al_2O_3 , hereafter referred to as alumina, to model the 11- μm feature in the PPN IRAS 22036+5306 (hereafter I22036).

Pre-solar grains separated from meteorites record an extensive AGB input to the Solar System. This is particularly evident from silicon carbide grains that mostly originate from AGB stars with $\text{C/O} > 1$. However, a small fraction of the AGB dust appears to be O-rich as evidenced by micrometer-sized Al_2O_3 with both amorphous alumina and corundum mineral structure (Stroud, Nittler & Alexander 2004). The rare pre-solar silicate grains (olivine) that have been found have similar oxygen isotopic compositions to the oxide grains (Messenger et al. 2003) indicating that oxide and silicate phases are probably abundant around AGB stars, and their low abundance relative to silicon carbide in meteorites suggests they are not preserved during transport to the protonebula, and/or during Solar System formation. Pre-solar silicon carbide grains generally have only moderate enrichments of ^{13}C relative to the solar $^{12}\text{C}/^{13}\text{C}$ ratio whereas Sahai et al. (2006) have measured the $^{13}\text{C}/^{12}\text{C}$ for I22036 and find it to be very high (0.16) near the limit for CNO-cycle nucleosynthesis (0.33), and consistent with a star of mass greater than $4M_{\odot}$. This is also consistent with the oxygen isotopic compositions of meteoritic corundum grains that are moderately depleted in ^{18}O but significantly enriched in ^{17}O which has been ascribed to hot-bottom burning in 4.5 to 7 M_{\odot} stars (Boothroyd, Sackmann & Wasserburg 1995).

The use of forms of Al_2O_3 as a grain species to explain the broadening of the 10- μm silicate feature to longer wavelengths in astronomical spectra is not new. Mitchell & Robinson (1978) modelled the spectrum of the high mass, high mass-loss rate variable Eta Carinae using a model based on the quasi-diffusion method of Leung (Leung 1975, 1976; see also Egan, Leung & Spagna 1988). Their best-fitting model used a mixture of forsterite (57 per cent), corundum (21 per cent) and iron (22 per cent), and was in excellent agreement with the spectral data available at that time for Eta Carinae over the entire wavelength range 0.36–35 μm . More recently, Speck et al. (2000) have modelled the broad 10- μm emission band seen towards oxygen-rich AGB stars using alumina and silicate dust.

In this paper, we present evidence for the existence of Al_2O_3 in the dust shell of I22036, a bipolar nebula with a thick dust torus obscuring the central star (Sahai et al. 2006). I22036 displays a deep 3- μm H_2O ice band and an unusual '10- μm ' band that actually peaks at 11 μm (Sahai et al. 2003). The *Infrared Space Observatory* (ISO) Short-Wavelength Spectrometer (SWS) and Long-Wavelength Spectrometer (LWS) spectra of this star have previously been modelled using bare amorphous silicate grains by Sahai et al. (2003). Of importance to the aims of this present study is the significant discrepancy in the fit of their model to the observed 11- μm band. These authors suggest that inclusion of H_2O ice in their model would improve the fit in this region. However, we have found this not to be the case and we propose a different explanation based on a mixture of alumina and olivine that leads to an excellent match to the observed 11- μm band.

This study is significant for two key reasons: firstly, the evidence for the presence of Al_2O_3 in I22036 strengthens the case for recent findings obtained in the context of similar high mass-loss rate stars

(close to the tip of the AGB and beyond). In our previous work (Maldoni et al. 2004, 2005), we have argued that Al_2O_3 is present as a distinct dust population throughout the dust envelope. Secondly, the alumina abundance required to fit the 11- μm band in I22036 is remarkably large. Referring to the quote above by Posch et al. (2003), the mineralogy of some low mass-loss stars appears to be significantly silicate-deficient. Our results are the first to indicate that this paradigm may also apply to some high mass-loss stars.

2 THE MODEL

In this work, we modelled the spectral energy distribution (SED) of I22036 using the publicly available code DUSTY developed by Ivezić & Elitzur (1997), which solves the spherical radiative transfer problem using the self-similarity and scaling behaviour of infrared (IR) emission from radiatively heated dust. To solve the radiative transfer problem including absorption, emission and scattering, several properties of the central source and its surrounding dust envelope are required, viz. (i) the spectral shape of the central source's radiation; (ii) the dust properties, i.e. the envelope's chemical composition and grain-size distribution as well as the dust temperature at the inner boundary; (iii) the relative thickness of the envelope, i.e. the ratio of outer to inner radius, R , and the density distribution, ρ , where $\rho \propto r^{-n}$ and (iv) the total optical depth at a given reference wavelength. Whilst this code precludes modelling of ice-mantled grains it does allow for an arbitrary number of consecutive shells to be easily set up, each of these being characterized by variable dust distribution power index and geometrical thickness parameters. The code also comes with an extensive library of optical constants of many species of astrophysical relevance.

For the modelling presented in this work, we have fixed the central source temperature at 6500 K which is in accordance with the F4 classification of I22036 (Sahai et al. 2003). Optical constants for Al_2O_3 alumina (porous sample, Begemann et al. 1997), and amorphous silicate of olivine composition (MgFeSiO_4 , Dorschner et al. 1995), hereafter olivine, were retrieved from the DUSTY optical library. As discussed later, models using other species were also generated but alumina and olivine were all that was required to obtain an excellent fit to the 11- μm band of I22036. The grain-size distribution was initially set to 0.005–0.25 μm (Mathis, Rumpl & Nordsieck 1977, hereafter MRN) and the lower bound was subsequently increased so as to optimize the model fits. As shown later, models employing larger grain sizes were also generated as these proved useful in fitting the far-IR segment of the observational data.

3 RESULTS

I22036 was observed by ISO using the SWS and LWS. We have retrieved this data from the ISO archive and have applied standard data reduction recipes to the spectra. The reduced ISO spectrum is shown in Fig. 1 along with a (subjectively defined) best-fitting model (*Model 1*) and the corresponding best-fitting parameters are presented in Table 1. Significantly, the alumina/olivine abundance (by number) required by *Model 1* is 70/30. Alumina/olivine dust mixtures heavily skewed towards olivine were initially used but proved substantially inadequate in fitting both the broadness and peak wavelength position of the 11- μm band, requirements that only alumina-dominated mixtures proved capable of fulfilling. The best-fitting model fits the data reasonably well across the near- and mid-IR spectral segments, particularly the 11- μm band, but the far-IR mismatch suggests that our model lacked large cold grains which are efficient emitters in this region. This disagreement is compounded

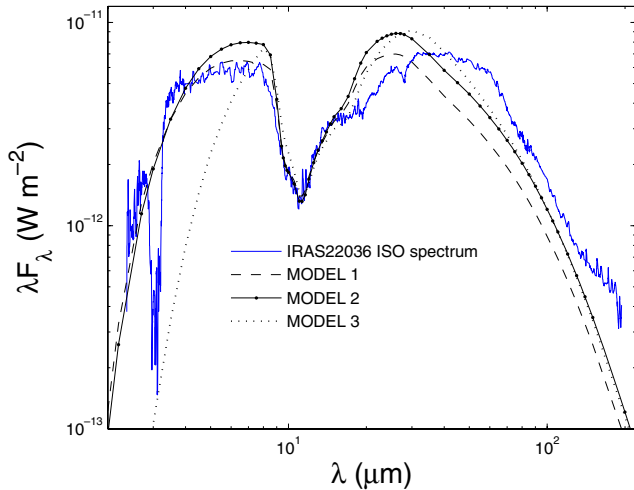


Figure 1. The ISO spectrum of IRAS 22036 (solid line) and the best-fitting model, *Model 1* (dashed line). Refer to Table 1 for the *Model 1* modelling parameters. Also shown are *Model 2* (solid line with dots) obtained with a slightly larger total optical depth ($\tau_{9.8} = 7.3$) than *Model 1*, and *Model 3* (dotted line) obtained with a larger grain-size upper limit ($5 \mu\text{m}$) than *Model 1*.

Table 1. Modelling parameters of the best-fitting model, *Model 1*, shown in Fig. 1. The total optical depth of the three shell configuration is $\tau_{9.8} = 6.2$. The assumed grain-size distribution is $0.1\text{--}0.25 \mu\text{m}$ and stellar temperature T_* is 6500 K. The alumina/olivine ratio (by number) is 70/30 per cent.

Shell	R	n	$T(\text{K})$
1	1–50	1.6	1500–119
2	50–80	1.3	119–99
3	80–1000	1.3	99–38

by the lack in *Model 1* of ice-coated grains as H_2O ice displays substantial emission in the $40\text{--}80 \mu\text{m}$ range in the form of a broad $44\text{-}\mu\text{m}$ band and an even broader one at $62 \mu\text{m}$ extending from about 50 to $80 \mu\text{m}$ (see e.g. Dijkstra et al. 2006).

Model 1 is the end-result of modelling which initially assumed the standard MRN grain-size distribution. However, we found that increasing the lower bound gave a better overall fit to the near- and mid-IR, particularly the $11\text{-}\mu\text{m}$ band (the best-fitting model was obtained with a $0.1\text{--}0.25 \mu\text{m}$ grain-size distribution). This is in agreement with previous work suggesting that the distribution of grains in dust shells of evolved stars appears to be peaked at a dominant size (Winters et al. 1997). Attempts to ameliorate the far-IR discrepancy using the adopted grain-size distribution were not successful. An improvement in the far-IR fit translated into a worsening in the near-IR fit (and vice versa) and a typical model, obtained with a slightly larger optical depth ($\tau_{9.8} = 7.3$) than that which yielded *Model 1*, is also presented in Fig. 1 (labelled *Model 2*). Similar results were obtained with models incorporating a large upper bound grain size ($5 \mu\text{m}$) and one such model is also shown in Fig. 1 (*Model 3*). The inclusion of these large grains, albeit a small number in view of the exponential nature of the dust distribution, only leads to a marginally better far-IR fit than *Model 2*, and produces a substantial drop in the modelled near-IR fluxes, showing that even larger grains can only compound this problem. It is very likely that

a proper treatment of the axisymmetric geometry of I22036 would allow the simultaneous presence of both small and very large grains (see e.g. Ueta & Meixner 2003).

The model setup yielding *Model 1* consisted of a hot ($1500\text{--}119 \text{K}$) shell, a warm ($119\text{--}99 \text{K}$) shell and a cool ($99\text{--}38 \text{K}$) shell. The respective dust density indices are $n = 1.6$ for the hot shell and $n = 1.3$ for both the warm and cool shells. In comparison to our modelling parameters shown in Table 1, Sahai et al. (2003) have implemented a dust configuration comprising a hot ($1000\text{--}350 \text{K}$) disc, a warm ($145\text{--}82 \text{K}$) shell and a cool ($67\text{--}35 \text{K}$) shell, all defined by an r^{-2} density law. A feature of DUSTY is that grain mixtures are simulated by a single-type grain constructed from an average of the respective optical properties. Furthermore, the DUSTY code assumes this single-type grain to be located throughout the entire radial grid. Therefore, in this sense, the alumina and olivine grains in our models are assumed to be co-spatial right throughout the three shells. Similarly, the temperature range, 1500K at the inner boundary to 38K at the outer one, refers to this single-type grain construct.

We note in passing that in order to check the validity of our best-fitting model, we have run a Leung (1975)-type model with essentially the same model parameters as those used for *Model 1* in DUSTY. The DUSTY and Leung-type model results were reassuringly similar.

The high upper temperature derived from the modelling shows that the near-IR fluxes are due to hot grains located within the inner dust regions. This would seem to suggest that the I22036 dust torus has not yet detached. However, this may be an artefact of our modelling setup. Recall above that Sahai et al. (2003) achieve a similar fit to the near-IR assuming an upper temperature of 1000K . The crucial parameter may be their use of an inner disc [modelled as an axially symmetric, wedge-shaped fraction (~ 0.4) of a sphere] as opposed to a spherical shell used in our modelling. As noted above, our model cannot simultaneously fit the near- and far-IR as it fails to account for the axial symmetry of I22036. Ueta & Meixner (2003) have developed a two-dimensional code which allows proper treatment of the axial symmetry of PPNs (an inner hot disc and an outer cooler spherically symmetric shell). Their models show that changes in the inclination angle of the axis of symmetry induce changes in the near-IR fluxes; for example, an edge-on disc results in higher near-IR fluxes (hotter grains) than a face-on configuration (cooler grains). The inference is that one-dimensional models of an inner shell necessarily only simulate the highest possible temperatures, comparable to an edge-on disc, and it is not possible to discriminate between attached and detached dust shells/tori.

Comparing our best-fitting model with that presented by Sahai et al. (2003) (see their fig. 3), we note that our model matches the near- and mid-IR data equally well (but not the far-IR) and, unlike Sahai et al., we achieve an excellent match to the $11\text{-}\mu\text{m}$ band. Sahai et al. suggest that the peculiar $11\text{-}\mu\text{m}$ bandshape could be attributed to the contribution of the librational band of H_2O ice. Certainly, the deep $3\text{-}\mu\text{m}$ band does imply substantial amounts of H_2O ice in the shell of I22036. However, in terms of the $11\text{-}\mu\text{m}$ band, this explanation is arguable as the observational evidence gathered thus far shows that the profile of the astronomical $10\text{-}\mu\text{m}$ dust band is only weakly sensitive (at best) to the presence of H_2O ice.

In a previous publication, Maldoni et al. (2004) showed that radiative transfer effects in the $10\text{-}\mu\text{m}$ silicate band considerably attenuate the librational band. This concerned spherically symmetric models of AGB and post-AGB stars and while it may be that in (axisymmetric) post-AGB stars orientation effects alter the strengths of the ice bands (Pontoppidan, Dullemond & van Dishoeck 2005), it is

difficult to imagine how this could compensate for the large discrepancy of the Sahai et al. model and the observed 11- μ m band. Not only is the librational band required to broaden the silicate band but also account for the considerable peak wavelength position shift from 10 to 11 μ m. It is worth recalling the example provided by W33a which has the deepest 3- μ m band of H₂O ice of any object observed thus far and yet its 10- μ m band profile does not reflect the presence of the 12- μ m ice band (see fig. 1 in Gibb et al. 2004).

The question of distinct alumina and silicate grain population versus composite grains was briefly explored in the context of alumina in OH231.8+4.2 (Maldoni et al. 2004). In that instance we used the radiative transfer code CSDUST3 of Egan et al. (1988) which, unlike DUSTY, treats multigrain components. The modelling indicated that there were clear differences between models assuming distinct dust populations and those assuming composite grains. Those assuming composite grains, obtained using the Maxwell-Garnett rule (Maxwell-Garnett 1904), proved to be inadequate in fitting the 10- μ m band of OH231.8+4.2 in that they did not yield enough opacity in the 10–15 μ m region.

In the case of OH231.8+4.2, the alumina abundance in the composite grains was limited to 30 per cent. This was the same alumina abundance required by the model assuming distinct dust populations which yielded an excellent fit to the 10- μ m band of OH231.8+4.2. Therefore, the composite grain models fail in the case of OH231.8+4.2 but yield a very good fit to the 11- μ m band of I22036. These seemingly contradictory results can be explained as follows. Fig. 2 in this work illustrates the effects of the contribution of alumina on the 10- μ m silicate band profile of I22036. Specifically, it shows models obtained with (i) 100 per cent olivine, (ii) 50 per cent olivine plus 50 per cent alumina and (iii) 30 per cent olivine plus 70 per cent alumina. As expected the olivine model peaks at 9.8 μ m and while the inclusion of 50 per cent alumina broadens the band, it does not alter the peak wavelength position. This can only be shifted to 11 μ m by including 70 per cent alumina. The reason why the composite model yields a good fit to the 11- μ m band of I22036, in contrast to the results obtained for OH231.8+4.2, is that the alumina abundance in the I22036 is so predominant that the best-fitting composite model (70 per cent alumina) approximates one assuming discrete alumina and olivine dust populations

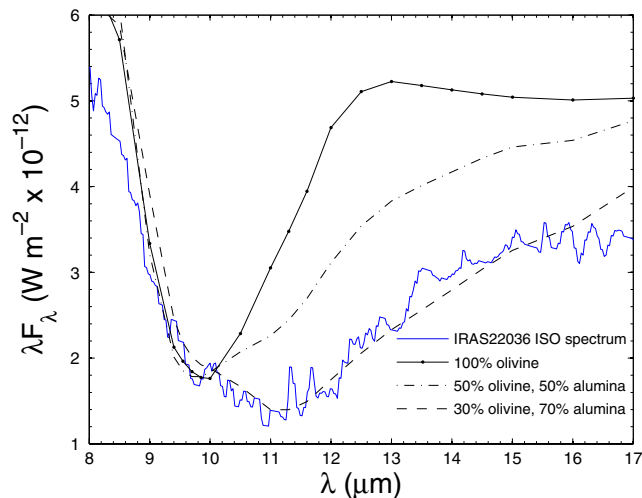


Figure 2. The mid-IR spectrum of IRAS 22036 (solid line). Also shown are models obtained using 100 per cent olivine (solid line with dots), 50 per cent each of olivine and alumina (dot-dashed line) and 30 per cent olivine, 70 per cent alumina (dashed line).

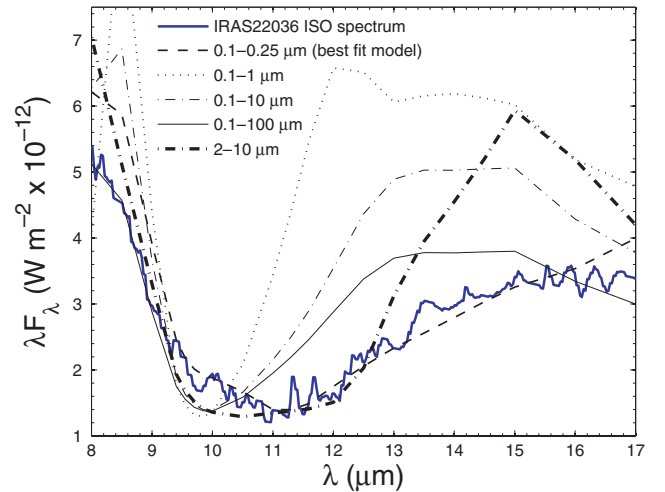


Figure 3. The effect of large grains on models. The shown are the mid-IR spectrum of IRAS 22036 (thick solid line) and olivine-only models obtained with grain-size distributions 0.1–1 μ m (dotted line), 0.1–10 μ m (thin dot-dashed line), 0.1–100 μ m (thin solid line) and 2–10 μ m (thick dot-dashed line). For comparison, the best-fitting model, *Model 1*, obtained with the olivine/alumina dust mixture is also shown (dashed line).

heavily skewed towards alumina. Based on our previous models of OH231.8+4.2 as well as a sample of OH/IR stars (Maldoni et al. 2005), which assumed distinct dust populations, we are confident that these also characterize the dust torus of I22036.

Condensation theory also predicts the formation of melilite (Ca₂Al₂Si₂O₇) (Tielens 1990) and models (not shown) incorporating melilite, olivine and alumina were also generated. While on the basis of these we cannot discount the presence of melilite in the shell of I22036, the peculiar 11- μ m band profile could only be modelled, once again, by dust mixtures strongly dominated by alumina (~60 per cent).

We have also explored the possibility that large grains may at least partly contribute to the unusual appearance of the 11- μ m band. It is known that the 10- μ m band of amorphous silicate grains is not very sensitive to shape effects whereas large grains decrease the contrast of the band with respect to the continuum (Bouwman et al. 2001), i.e. large grains tend to emit/absorb like blackbodies with little in the way of spectral features characteristic of dust composition. In order to explore the impact of large grains in our modelling, Fig. 3 presents a comparison of the observed I22036 11- μ m band and models obtained with olivine dust-grain distributions of 0.1–1, 0.1–10, 0.1–100 and 2–10 μ m. Inspection of Fig. 3 shows that while the synthetic 10- μ m band becomes broader with increasing grain size it none the less fails to reproduce the long wavelength wing of the astronomical 11- μ m band. On this basis, we conclude that although the far-IR mismatch in Fig. 1 suggests the presence of grains larger than the adopted grain-size distribution, these can only partially contribute to both the broadness and the shift longwards of 10 μ m of the mid-IR band usually located at 9.8 μ m. Both the sharpness of the observed 11- μ m band and the significant near-IR mismatch resulting from the large grain modelling point to the dust composition being a key parameter in determining the profile of the 11- μ m band.

Studies have shown that crystalline silicates are present in dust shells of O-rich stars (Kemper et al. 2001; Molster, Waters & Tielens 2002). Of these, forsterite (Mg₂SiO₄) is a seemingly promising candidate as the carrier of the 11- μ m band in I22036 as in the region

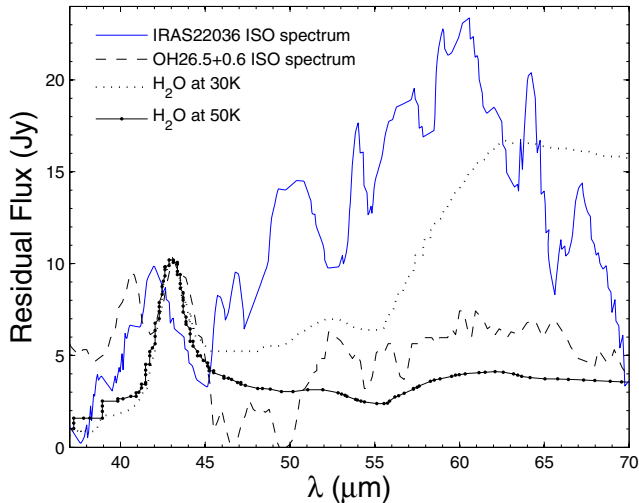


Figure 4. The far-IR spectrum of IRAS 22036 (solid line) overlaid on that of OH26.5+0.6 (dashed line). Also shown is the emission spectrum of H₂O ice at 30 K (dotted line) and 50 K (solid line with dots). Comparing the IRAS 22036 and OH26.5+0.6 spectra, note the absence in the IRAS 22036 spectrum of a double-band structure in the 40–45 μm range. Also note the enhanced strength of the 60- μm emission band in the IRAS 22036 spectrum.

of interest it has bands at 11 and 10 μm . However, given the strength of the astronomical 11- μm band, we would expect that if this were the case there ought to be corresponding (significant) substructure at 10 μm . The latter is not detected and based also on the usually modest abundances of crystalline silicates, as well as the analysis of the far-IR spectrum (see later), we do not believe forsterite to be a significant contributor to the 11- μm band.

In order to probe the unusually high abundance of alumina suggested by the modelling, we have examined the spectrum of I22036 for other spectral features that may support (or contradict) our results. This process is hampered by the fact that alumina has only one IR band. However, useful clues on the dust condensation process in I22036 can be obtained by analysing bands due to other dust species. To that end, we have fitted an arbitrary continuum to the SED shown in Fig. 1 so as to highlight the far-IR spectral features. The resulting continuum-subtracted spectrum is shown in Fig. 4. In the same figure, we have compared this data with that of a more ‘typical’ O-rich AGB star, OH26.5+0.6. In contrast to OH26.5+0.6, the 60- μm emission band is the most dominant feature in the spectrum of I22036 and we attribute this to the 62- μm band of H₂O ice. Laboratory studies have shown that very cold H₂O ice emits more efficiently at 62 μm rather than 44 μm (Bertie, Labbè & Whalley 1969). This is demonstrated by comparison of the 30 and 50 K H₂O ice emission spectra (Bertie et al. 1969), also presented in Fig. 4, showing an enhanced 62- μm band in the 30 K spectrum. Furthermore, laboratory results of Smith et al. (1994) have shown that the peak wavelength position of the 44- μm band of crystalline H₂O ice shifts from 44.7 μm at 140 K to 42.7 μm at 10 K. I22036 displays both a band at 42 μm and a prominent one at 60 μm ; therefore, on the basis of these spectral attributes, we surmise that the bulk of H₂O ice in I22036 must be very cold.

The other striking feature of I22036 is, compared to OH26.5+0.6, its spectrum displays only one peak in the 40–45 μm interval, as opposed to two. Bands at 40 and 43 μm occur quite frequently in the spectra of O-rich AGB stars (see Molster et al. 2002 for a comprehensive study of the astronomical crystalline bands). Both enstatite

(MgSiO₃) and diopside (CaMgSi₂O₆) have a band at around 40.5 μm with enstatite also displaying one at 43 μm . I22036 displays only a 43- μm band and, at best, shoulders at 41 and 44 μm . The absence of these crystalline silicate bands suggests a condensation process in I22036 which differs in some details from those leading to dust formation in other similar stars (at least as judged by the frequent occurrence of the two bands in the 40–45 μm range).

4 DISCUSSION

Sahai et al. (2006) have proposed that the observed fluxes at 0.88 and 2.6 mm require the presence of large cold grains with diameters greater than 1 mm. Such large grains require that condensation is extensive and ongoing and that grains are protected from degradation, probably within the torus. However, modelling here indicates an extremely high temperature in the inner region of the torus.

The composition of the grains appears to be consistent with an oxygen-rich gas composition (i.e. C/O < 1). However, the results presented here indicate that the mineralogy of I22036 is oxide dominated, rather than silicate dominated as appears typical for AGB stars with low C/O. Our detailed modelling of the spectra around 11 μm reveals that silicate alone, or silicate with H₂O ice, cannot produce the shift of the 10- μm to 11- μm . From considerations of the condensation sequence, and an extremely well-fitted spectrum, alumina mixing with subordinate silicate provides the best fit to the observed features. But, not only is alumina present, it also dominates over the silicate contribution with a 70:30 mixing ratio.

During condensation of O-rich circumstellar gas (Lodders & Fegley 1999), it is expected that Al₂O₃ will be the first solid phase. Condensation of Ca–Al–Ti oxides and silicates follows, before condensation of Mg silicates. Around C-rich stars, SiC and graphite are the first condensates with Al condensation suppressed until AlN is stable at much lower temperatures. However, AlN is a significant substituting molecule in meteoritic SiC indicating that a fraction of Al can and does condense at higher temperature.

Early forming condensates can follow two different pathways. In equilibrium condensation, they should react with the gas in the stabilization of lower temperature minerals. Hence, solid Al₂O₃ will react with the gas at lower temperatures to form hibonite (CaAl₁₂O₁₉), and then melilite (Ca₂Al₂Si₂O₇). The expanding gas shell from a star probably cannot maintain equilibrium in the gas and so early forming condensates would become coated and encapsulated in lower temperature condensates. A classical pathway is illustrated in OH26.5+0.6. This spectrum consists solely of silicate absorption features indicating that Al₂O₃ has been resorbed during condensation, or that it has been encapsulated in silicate. In either case, Al₂O₃ is not visible.

In the case of I22036, both the large alumina/olivine abundance ratio and the lack of a 41- μm band are strong evidence that the condensation sequence has not followed a classical condensation scheme. In this case, the signature of Al₂O₃ is maintained. From our modelling, the inner toroid of the disc is at an extremely high temperature (1500 K). At this temperature, Al₂O₃ is condensing from the gas and stabilizing into dust grains. However, silicate will not condense until the gas has moved further away from the star to lower temperatures. In this case, silicate dust growth may be inhibited because the gas density is falling too quickly for nucleation to occur. If this is the case, the high alumina/silicate ratio for I22036 is a natural consequence of its high temperature.

A complicating factor in condensation around an AGB star is that a common evolutionary trend is for the star to evolve to more C-rich compositions as dredge-up occurs and so the Al chemistry could be

a sensitive indicator to C/O chemistry of the star. As the oxygen-rich star becomes more C-rich, it is possible that Al will essentially scavenge all available oxygen and then the silicate condensation will again be suppressed.

There is a general consensus in the literature that Al_2O_3 is intimately linked with the dust formation process in low mass-loss stars (see the comprehensive work of Speck et al. 2000). TiO is also considered to be of primary importance in the formation of early condensates (Jeong, Winters & Sedlmayr 1999), however, the solar abundance of Ti is a factor of 20 lower than Al, and Ti can be substituted into corundum. The evidence for circumstellar alumina is primarily based on models of the broad emission feature at about 11.5–12 μm . The anomalous nature of this feature has been recognized in classes SE1–SE3 of the scheme of Sloan & Price (1995). These authors have classified oxygen-rich AGB 10- μm band spectra according to the ratios of the 12- and 11- μm fluxes, F12/F11 and the 11- and 10- μm fluxes, F11/F10. On the basis of these flux ratios, they have then assigned a spectral index SE to each class. The broadness of the 10- μm band in classes SE1–SE3 suggests the presence of alumina. Speck et al. (2000) classified this feature as AGB ‘broad’. In both these schemes, the initial broad 11.5- μm band is a representative of a silicate/alumina mixture dominated by the latter species. As the dust evolves the silicate, signature becomes more prominent until finally the bandshape resembles the ‘classic’ 10- μm silicate band, pointing to a silicate-dominated mineralogy.

In the scheme of Sloan & Price (1995), the 11- μm band detected in the spectrum of I22036 is then typical of the SE1–SE3 spectral profiles, albeit in a high mass-loss rate scenario. This too suggests that the dust condensation process was terminated quite early in the expected sequence. Our results highlight the significance of Al_2O_3 in the dust formation process throughout the AGB phase and, importantly, also strengthen evidence for its presence in dust shells of highly evolved stars (i.e. near and beyond the tip of the AGB). Recent studies have presented similar evidence for the massive ($>9 M_\odot$) post-AGB stars Betelgeuse (Verhoelst 2005) and Eta Carinae (Chesneau et al. 2005). Verhoelst finds strong evidence of a thin layer of alumina grains very close to the photosphere in Betelgeuse. Furthermore, the observational data gathered by Verhoelst suggest that the Al_2O_3 may be formed within the photospheric H_2O layer and that there is a significant gap between the Al_2O_3 and silicate dust condensation regions. Al_2O_3 dust is present in this gap region but due to the low density and temperature factors it is undetectable. These findings give credence to those dust condensation schemes which begin with the early condensation of Al_2O_3 grains which then ‘spawn’ the silicate dust grains (Salpeter 1977; Sedlmayr 1989; Tielens 1990; Lodders & Fegley 1999).

The work of Chesneau et al. (2005) is of particular significance as their models of *N*-band spectra obtained in different regions of the Eta Carinae nebula show evidence that the mineralogy of some of the ejected dust clouds is dominated by Al_2O_3 . It is noteworthy that even the silicate-dominated models require substantial amounts of alumina in order to fit the spectra. These authors attribute the presence of Al_2O_3 -dominated dust clouds to factors such as low-oxygen abundance or insufficient gas density in the outflow, both of these leading to a condensation freeze out. We note that strong evidence for such an abrupt termination of dust condensation in low mass-loss rate AGB stars has recently been presented by Heras & Hony (2005).

Although it appears that Al_2O_3 is an important dust component in the ejecta of highly evolved O-rich stars it is still not clear why I22036 alone thus far displays an 11- μm band (and such a large alumina abundance). It is instructive to compare this star with M1–92

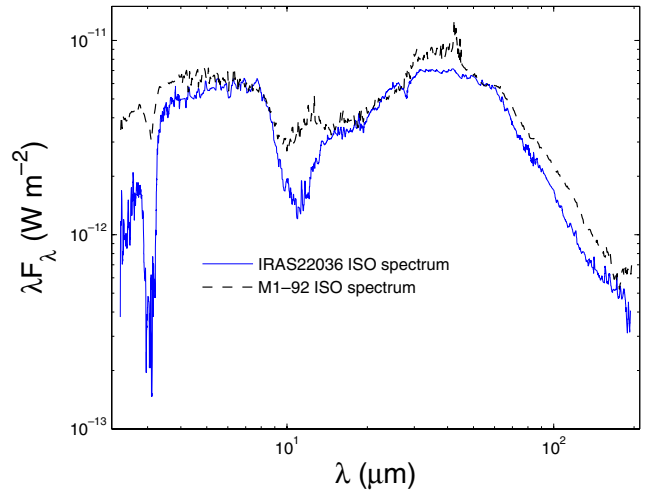


Figure 5. The *ISO* spectra of IRAS 22036 (solid line) and M1–92 (dashed line). The M1–92 spectrum has been shifted to best match the near- and far-IR fluxes from IRAS 22036.

which is more evolved but, similarly to I22036, still displays a 3- μm ice band. The two respective SEDs are overplotted in Fig. 5, the SED of M1–92 having been shifted to match the near- and far-IR fluxes of I22036. The comparison shows an excellent agreement between the respective 20- μm band regions and at longer wavelengths. It also highlights the striking difference between the 11- μm band of I22036 and the more ‘normal’ 10- μm band of M1–92, particularly given the remarkably similarity of the respective 20- μm bands. We also note the substantial opacity between the 10- and 20- μm bands in M1–92. This may be due to radiative transfer effects or may be due to a species such as alumina. Given the results of this work we suggest the latter is probably the case.

Is the 11- μm band of I22036 indicative of a quick and transient stage along the path to the PN phase, or has the dust been Al_2O_3 rich as far back as the early AGB phase? Could it be an orientation effect of the I22036 torus? We note that Molster et al. (1999) comment that ‘the 10- μm band in AFGL4106 is significantly redshifted compared to the bump found in most O-rich (post-)AGB stars’. The band in AFGL4106 is an emission feature and may either be the emission counterpart of the 11- μm absorption band in I22036 or due to dust processing taking place in PPNs and PNs (see e.g. Speck & Hofmeister 2004). *Spitzer* data and two-dimensional modelling are needed to probe the spatial distribution of Al_2O_3 dust in this and other PPNs/PNs. Unlike *ISO*, the spectral coverage of *Spitzer* is limited to 40 μm . However, its superior sensitivity and spatial resolution compared to *ISO* means that *Spitzer* data at up to this cut-off wavelength are likely to yield many useful clues on the mineralogy of highly evolved stars such as PPNs/PNs and, in particular, on the relationship of Al_2O_3 to other dust species.

5 CONCLUSIONS

Radiative transfer modelling of the *ISO* spectrum of I22036 has shown that the broad 11- μm band in I22036 can be modelled with an alumina/olivine mixture substantially dominated by the former. Alumina dominates the dust makeup to the extent that it shifts the observed mid-IR band from the usual 9.8- μm peak wavelength position to 11 μm . The results of this work add further credence to recent findings on the presence of Al_2O_3 in evolved stars, namely

that significant amounts of Al_2O_3 may be present in shells of stars near or beyond the tip of the AGB.

There is observational evidence suggesting that stars in the early stages of the AGB phase, where the mass-loss rate is low, have dust shells that are oxide dominated. The results presented here suggest that for some stars the dust mineralogy may not switch to a silicate-dominated composition. In the case of I22036, the overabundance of Al_2O_3 appears to be a result of the extremely high temperatures in the inner torus region where Al_2O_3 is a stable condensing phase and it is too hot for condensation of silicate. As the gas moves out to a temperature regime where silicate grains could condense, nucleation is inhibited by the rapid decline in gas density.

ACKNOWLEDGMENTS

We thank the referee, Angela Speck, for valuable comments which we believe have led to the substantial improvement of this paper, and also Peter Wood for useful discussions on AGB stars. MMM acknowledges a visiting fellowship at the School of Physical, Environmental and Mathematical Sciences, Australian Defence Force Academy, Canberra. This work was supported by an ARC Discovery Grant.

REFERENCES

- Begemann B., Dorschner J., Henning Th., Mutschke H., Guertler J., Koempe C., Nass R., 1997, *ApJ*, 476, 199
- Bertie J. E., Labbè H. J., Whalley E., 1969, *J. Chem. Phys.*, 50, 4501
- Boothroyd A. I., Sackmann I.-J., Wasserburg G. J., 1995, *ApJ*, 442, L21
- Bouwman J., Meeus G., de Koter A., Hony S., Dominik C., Waters L. B. F. M., 2001, *A&A*, 375, 950
- Chesneau O. et al., 2005, *A&A*, 435, 1043
- DePew K., Speck A., Dijkstra C., 2006, *ApJ*, 640, 971
- Dijkstra C., Speck A. K., 2006, *ApJ*, 651, 288
- Dijkstra C., Dominik C., Bouwman J., de Koter A., 2006, *A&A*, 449, 1101
- Dorschner J., Begemann B., Henning T., Jaeger C., Mutschke H., 1995, *A&A*, 300, 503
- Egan M. P., Leung C. M., Spagna G. F., 1988, *Comput. Phys. Commun.*, 48, 271
- Gibb E. L., Whittet D. C. B., Boogert A. C. A., Tielens A. G. G. M., 2004, *Ap&SS*, 151, 35
- Heras A. M., Hony S., 2005, *A&A*, 439, 171
- Ivezic Z., Elitzur M., 1997, *MNRAS*, 287, 799
- Jeong K. S., Winters J. M., Sedlmayr E., 1999, in Le Bertre T., Lèbre A., Waelkens C., eds, *Proc. IAU Symp. 191, Asymptotic Giant Branch Stars*. Astron. Soc. Pac., San Francisco, p. 233
- Kemper F., Waters L. B. F. M., de Koter A., Tielens A. G. G. M., 2001, *A&A*, 369, 132
- Kwok S., 1993, *ARA&A*, 31, 63
- Leung C. M., 1975, *ApJ*, 199, 340
- Leung C. M., 1976, *J. Quant. Spectrosc. Radiative Transfer*, 16, 559
- Lodders K., Fegley B., 1999, in Le Bertre T., Lèbre A., Waelkens C., eds, *Proc. IAU Symp. 191, Asymptotic Giant Branch Stars*. Astron. Soc. Pac., San Francisco, p. 279
- Maldoni M. M., Egan M. P., Robinson G., Smith R. G., Wright C. M., 2004, *MNRAS*, 349, 665
- Maldoni M. M., Ireland T. R., Smith R. G., Robinson G., 2005, *MNRAS*, 362, 872
- Malthis J. S., Rimpl W., Nordsieck K. H., 1977, *ApJ*, 217, 425 (MRN)
- Maxwell-Garnett J. C., 1904, *Phil. Trans. R. Soc. Lond. A*, 203, 385
- Messenger S., Keller L. P., Stadermann F. J., Walker R. M., Zinner E., 2003, *Sci*, 300, 105
- Mitchell R. M., Robinson G., 1978, *ApJ*, 220, 841
- Molster F. J. et al., 1999, *A&A*, 350, 163
- Molster F. J., Waters L. B. F. M., Tielens A. G. G. M., 2002, *A&A*, 382, 222
- Nuth J. A., III, Hecht J. H., 1990, *Ap&SS*, 163, 79
- Posch T., Kerschbaum F., Mutschke H., Fabian D., Clement D., Dorschner J., 2002, in Gry C., Peschke S. B., Matagne J., Garcia-Lario P., Lorente R., Salama A., eds, *ESA SP-511, Exploiting the ISO Data Archive-Infrared Astronomy in the Internet Age*. ESA Publications Division, Noordwijk, p. 141
- Pontoppidan K. M., Dullemond C. P., van Dishoeck E. F., 2005, *ApJ*, 622, 463
- Sahai R., Zijlstra A., Sánchez Contreras C., Morris M., 2003, *ApJ*, 586, L81
- Sahai R., Young K., Patel N. A., Sánchez Contreras C., Morris M., 2006, *ApJ*, 653, 1241
- Salpeter E. E., 1977, *ApJ*, 193, 585
- Sedlmayr E., 1989, in Allamandola L. J., Tielens A. G. G. M., eds, *Interstellar Dust*. Kluwer, Dordrecht, p. 467
- Sloan G. C., Price S. D., 1995, *ApJ*, 451, 758
- Smith R. G., Robinson G., Hyland A. R., Carpenter G. L., 1994, *MNRAS*, 271, 481
- Speck A. K., Hofmeister A. M., 2004, *ApJ*, 600, 986
- Speck A. K., Barlow M. J., Sylvester R. J., Hofmeister A. M., 2000, *A&AS*, 146, 437
- Stencel R. E., Nuth J. A., III, Little-Marenin I. R., Stephen J., 1990, *ApJ*, 350, L45
- Stroud R. M., Nittler L. R., Alexander C. M. O'D., 2004, *Sci*, 305, 1455
- Tielens A. G. G. M., 1990, in Menessier M. O., Omont A., eds, *From Miras to Planetary Nebulae, Which Path for Stellar Evolution?* Editions Frontières, France, p. 186
- Ueta T., Meixner M., 2003, *ApJ*, 586, 1338
- Vassiliadis E., Wood P. R., 1993, *ApJ*, 413, 641
- Verhoelst T., 2005, PhD thesis, K. U. Leuven
- Winters J. M., Fleischer A. J., Le Bertre T., Sedlmayr E., 1997, *A&A*, 326, 305

This paper has been typeset from a $\text{T}_{\text{E}}\text{X}/\text{L}^{\text{A}}\text{T}_{\text{E}}\text{X}$ file prepared by the author.